LA-3997

LOS ALAMOS SCIENTIFIC LABORATORY
of the
University of California
LOS ALAMOS • NEW MEXICO

Resonant Final State Interactions in $^{3}He(d,tp)^{1}H$, $^{2}H(t,tp)n$, and $^{3}H(d,tp)n$ Reactions

UNITED STATES
ATOMIC ENERGY COMMISSION
CONTRACT W-7405-ENG. 36

This report expresses the opinions of the author or authors and does not necessarily reflect the opinions or views of the Los Alamos Scientific Laboratory.

Printed in the United States of America. Available from
Clearinghouse for Federal Scientific and Technical Information
National Bureau of Standards, U. S. Department of Commerce
Springfield, Virginia 22151
Price: Printed Copy $3.00; Microfiche $0.65

LA-3997
UC-34, PHYSICS
TID-4500

LOS ALAMOS SCIENTIFIC LABORATORY
of the
University of California
LOS ALAMOS • NEW MEXICO

Report written: August 27, 1968
Report distributed: November 25, 1968

Resonant Final State Interactions in $^{3}He(d,tp)^{1}H$, $^{2}H(t,tp)n$, and $^{3}H(d,tp)n$ Reactions

by

R. W. Newsome, Jr.*

*Present address: Bellcomm, Inc., Washington, D. C.

RESONANT FINAL STATE INTERACTIONS IN $^{3}He(d,tp)^{1}H$, $^{2}H(t,tp)n$, and $^{3}H(d,tp)n$ REACTIONS

by

R. W. Newsome, Jr.

ABSTRACT

A kinematically unique two-parameter experiment was used to search for resonant interactions between pairs of particles in the three-body final states of the reactions studied. The center-of-mass excitation range was from 20.5 to 29.3 MeV above the ^{4}He ground state for the t + p system, and from 21.0 to 29.1 MeV above the ^{4}He ground state for the t + n system. The reaction $^{3}He(d,tp)^{1}H$ with 15-MeV incident deuterons yielded a distinct resonance in the t + p system at 21.5 ± 0.1 MeV, with a width of approximately 1 MeV. For this same reaction with 20-MeV incident deuterons, the peak cross section for this t + p resonance shifted to 22.0 ± 0.2 MeV, with a width of approximately 2 MeV. There is weak evidence that this latter resonance can be resolved into resonances at approximately 21.6 and 22.2 MeV. Data from the reaction $^{3}H(d,tp)n$, which were obtained with 20-MeV incident deuterons, are also consistent with the existence of a broad resonance in the t + p system at approximately 22 MeV above the ^{4}He ground state. The reaction $^{2}H(t,tp)n$ was run with 21-MeV tritons; however, the breakup spectra are unfortunately dominated by phase space and the spectator pole-type breakup of the deuteron. Evidence for other possible resonances is inconclusive.

INTRODUCTION

Recent experimental[1-6] and theoretical[7-10] studies of four-nucleon systems have resulted in the identification of an unexpectedly large number of virtual states.[11,12] Most of the quantitative information concerning the existence and properties of these resonances has been deduced from phase-shift analysis of reactions which leave two particles in the final state.[13-19] In principle, it should be possible to completely describe these resonances in terms of extensive phase-shift analyses. In practice, however, it is often not feasible to obtain the comprehensive set of data required for uniqueness.

Reactions which lead to three particles in the final state are much more complicated both theoretically and experimentally. In general, however, the center-of-mass excitation energy of resonant two-particle final-state interactions may be determined, to within the resonant half-width, via kinematically unique two-parameter measurements of three-particle breakup reactions. The

yield of quantitative spectroscopic information from such measurements is currently inhibited by lack of adequate understanding of the interplay between the reaction mechanisms and the final-state interactions. Nevertheless, the two-particle resonances observed by means of these more complicated three-particle breakup reactions are potentially very useful as both a check of and a challenge to predictions based on interpretations of the simpler two-body breakup reactions.

The work described here was first reported in Ref. 20. It is the result of kinematically unique two-parameter measurements of several three-body breakup reactions. A search was made for center-of-mass energy-invariant enhancements in the measured cross sections corresponding to resonant interactions between any two of the three breakup particles. The range of excitation energies covered by these measurements for the t + p system extended from 0.7 MeV, just above the well-confirmed first excited state in ^{4}He which is approximately 0.2 MeV above the t + p breakup, to approximately 9.5 MeV above the t + p threshold. The corresponding excitation range for the t + n system extends from about 0.5 to about 8.5 MeV above the t + n rest mass.

Several of the three-body final-state systems considered have also been investigated in other one- and two-parameter experiments.[1-6] In particular, the detection of only one of the three breakup particles has been damonstrated to be extremely sensitive to two-particle resonance formation at low excitation above the t + p breakup threshold.[5,6] The corresponding resonance of the first excited state in ^{4}He is narrow enough so that the state of the final system is effectively two, and not three, particles.[2,5,6] A kinamatically unique two-parameter experiment is, however, much more sensitive to resonance formation at high excitation where resonances are expected to be very wide, corresponding to very short interaction times.

EXPERIMENTAL METHOD

A 3.8-cm-diam gas target was used. This target and the ΔE-E particle detection telescopes were inside a 51-cm-diam vacuum chamber. The entrance and exit beryllium foils for the gas target were, respectively, 25 and 13 μ thick. Target pressures were typically 300 mm of Hg. Beams of 15.21- and 20.175-MeV deuterons, and 21.35-MeV tritons were obtained from the Los Alamos three-stage tandem Van de Graaff facility. The beam intensity was varied from 50 to 300 nA, with the lower rates for small detector angles used to avoid pulse pileup. No corrections were made for energy loss in the target gas because thie loss was generally comparable to the small uncertainty in energy loss due to the approximately 10% uncertainty in the exit window thickness.

The ΔE-E counter telescopes were solid-state detectors. The E detectors were 2000-μ thick lithium-drifted silicon or, alternatively, several surface barrier detectors were ganged to produce the required stopping power. The ΔE detectors were surface barrier types 50- or 100-μ thick. These ΔE detectors were either oriented or mounted at 15° to minimize channeling. For several of the data runs, only one ΔE-E telescope in conjunction with a single E detector was required to uniquely identify both particle masses because the two-parameter coincidence requirement uniquely resolved the kinematic locus of interest. For high counting rates, however, a redundant mass identification with ΔE-E telescopes on both detection systems was useful in eliminating chance coincidences in the mass selection circuits.

The outputs of the ΔE-E telescopes were fed into analog computers[21] which, in conjunction with appropriate differential discriminators and slow coincidence circuits, are referred to as mass identifiers in Fig. 1. The fast coincidence timing circuits were zero-crossover units whose outputs were fed into a time-to-pulse-height converter. The timing resolution over the full range of pulse-height amplitudes was approximately 40 nsec. This was more than adequate because the angles were chosen so that the elastic background was off-scale in the two-parameter plane of interest. Chance coincidence corrections were generally less than 15% of the primary data.

The output of the time-to-pulse-height converter was then fed into two differential discriminators. The outputs from these discriminators were summed and used to gate a RIDL 256-channel analyzer. As shown in Fig. 1, this analyzer was used to monitor the integral number of "true" and "chance" events.

The ΔE-E signals were also summed and gated with a slow coincidence requirement between the output of the mass identifier and a "true" or "chance" output from the time-to-pulse-height converter. The gains for the ΔE and E signals were balanced, and the energy scales for the sum ΔE+E were calibrated by elastic scattering. These energy scales were cross-checked for consistency with the loci of the two-parameter data for several sets of angles. The "zero" for the angular settings was determined by requiring equal elastic scattering intensity on both sides of the beam.

The quality of the mass identification was constantly monitored with a storage oscilloscope. The vertical axis of the display was proportional to the energy, E, and the horizontal axis was proportional to the mass. This time-integrating display was most useful for setting discriminators and for detection of counter deterioration.

The output from the "chance" discriminator was used to route the chance events into a separate 64×64-channel array in the mamory bank of an SDS-930 on-line computer. To conserve the storage space in the available 12 k memory bank, the standard 24-bit words were split in half, with the true events in the first half of each word and the chance events routed into the bottom half. In this manner two 64×64 arrays could be stored with only 4 k words from the memory bank.

A computer program was written for the on-line SDS-930 computer which permitted the following major options: 1. storage of the original data on a high speed magnetic tape, 2. a two-dimensional computer-controlled display, and 3. a print-out of any of three 64×64-channel data arrays in 45 sec. The three possible data arrays are (a) the "true" array, (b) the "chance" array, and (c) the net array obtained by computer subtraction of the "corrected chance" array from the "true" array. The "corrected chance" array is the product of the "chance" array multiplied by a scaling factor which is unity if the widths of the "true" and "chance" gates are equal.

A supplementary computer program was often used for more detailed analysis. This program permitted the computer to take the "chance" corrected data from a storage tape and make the projected data sums on the horizontal and vertical axes. The energy calibrations for the two axes were also fed into the computer. This program then permitted the computer to calculate, channel by channel, the complete kinematics for the three-body breakup reaction of interest. The program was based on the composite summary of the appropriate kinematic equations by Ohlsen.[22] The projected data for both reactions could also be plotted with error flags obtained from the counting statistics. Complete print-outs of the "chance" corrected-data array and plots of these projected data along with complete kinematic analyses were thus available approximately 5 min. after any run.

DATA ANALYSIS

The data and some of the kinematic curves are presented in Figs. 2 through 18. The measurament of absolute cross sections was not an original goal of these exploratory experiments, but the data appeared consistent enough to justify such a determination. In making the solid-angle corrections, it was consistent with the accuracy of the data to use only the first-order terms from the analysis procedure formulated by Silverstein.[23] A graphical integration was made of the intersection of the beam and the active volumes defined by the collimators for the two detection systems. The size and location of the beam spot were determined with burns on photographic print paper, and the beam collimators were then adjusted to conform to and maintain this beam configuration. Optical techniques were used to align the detector collimators to less than half a degree.

In the relevant kinematic equations, the three particles in the final state are designated by the numerals 1, 2, and 3. The center-of-mass interaction energy for the particle pair (2,3) is given by[22]

$$E23 = E^c_{tot} - (m_1+m_2+m_3)E^c_1/(m_2+m_3), \quad (1)$$

where E^c_{tot} represents the total center-of-mass energy, and E^c_1 is the center-of-mass energy of particle 1. The other alternatives (i.e., E31 and E12) are obtainable by permuting the subscripts in Eq. (1).

The linear density of states projected along the E_1 energy axis is given by[22]

$$\rho_1(E_1)dE_1\Omega_1 d\Omega_2 = \frac{h^{-6} m_1 m_2 m_3 p_1 p_2 dE_1 d\Omega_1 d\Omega_2}{(m_2+m_3)+[m_2(\underline{p}_1-\underline{P})\cdot\underline{p}_2]/p_2^2}, \quad (2)$$

where $\underline{P} = \underline{p}_1 + \underline{p}_2 + \underline{p}_3$, and $d\Omega_1$ and $d\Omega_2$ are the solid angles subtended by the two detection systems.

Let us now assume that the differential cross section for projection along the E_1 axis is of the form[22]

$$\frac{d^2\sigma}{d\Omega_1 d\Omega_2 dE_1} = \frac{2\pi\mu_p}{\hbar^2 k_p}|\underline{M}|^2\rho_1(E_1), \quad (3)$$

where μ_p and k_p are, respectively, the mass and momentum for the incident projectile; $\underline{M}$ represents the nuclear matrix elements; and $\rho_1(E_1)$ is the projected phase space on the E_1 axis. In the simplest approximation, the matrix $\underline{M}$ is independent of E_1. For such a situation, the measured cross section divided by phase space should be a constant.

The Reaction ^{3}He(d,tp)^{1}H

The data for this reaction are shown in Figs. 2, 4, and 6 through 9. The incident deuteron energy, after correction for loss in the entrance foil, is 15 MeV for Figs. 2 and 4 and 20 MeV for Figs. 6 through 9. These data have been corrected for chance events, and the vertical error bars are based on counting statistics.

In Figs. 2 and 4, the solid curves were obtained by dividing the measured data points by the appropriate phase-space function. A smooth curve was then drawn with an arbitrary vertical scale factor.

Owing to beam misalignment, the absolute cross sections, on the right-hand vertical scale, have large errors ($\simeq \pm 70\%$). However, the relative cross sections for the four curves in Figs. 2 and 4 are believed to be accurate to within ±20%. The beam was well centered for the other data runs, and absolute errors were subsequently reduced to approximately ±30%.

In Figs. 2 and 4, arrows A, B, C, and D represent the approximate centroid of the broad resonant curves. Arrows 21.6 and 22.2 indicate center-of-mass excitation energies in MeV above the ground state of ^{4}He. The unbracketed numbers indicate the center of mass of the particle pair (1,2), whereas the numbers in parentheses indicate the center of mass of the pair (3,1). The symbol E3L(MIN) indicates a minimum in the laboratory energy of the unobserved particle (i.e., 3). The importance of this quantity will be noted later. The symbol ρ(MAX) indicates a maximum in the projected phase space.

In Fig. 3, the lab energy of the third particle is plotted on the right-hand vertical scale, and the left-hand vertical scale designates the center-of-mass excitation energies of the three different sets of final-state particle pairs. The outgoing particles in the final state are labeled 1, 2, and 3 for the triton and the two protons, respectively. Arrows marked A, B, C, and D refer to the approximate maxima in the cross sections for the curves in Fig. 2. Of the three center-of-mass energies, ΔE12 has the smallest magnitude, corresponding to the different positions of the four resonant maxima. The particle pair (2,3), corresponding to the two protons, has a very large energy ΔE23, which makes it an unlikely candidate. Although ΔE31 is relatively small, subsequent data at higher incident deuteron energy can be used to verify the choice of E12 as the appropriate interaction energy pair. The average E12 position for these maxima is 21.5 ± 0.1 MeV above the ^{4}He ground state. This agrees extremely well with the phase-shift predicted value[14] of 21.6 MeV. Note that the t + p rest mass is 19.81 MeV above the ^{4}He ground state. The data taken at the smallest angles in both Figs. 2 and 4 also tend to confirm the existence of a second level at approximately 22.2 MeV. There is further evidence for this level in the higher energy data.

In Fig. 5, the projection on the proton laboratory energy axis, E2L, is plotted. In place of the curves for E3L, which were plotted in Fig. 3, are the kinematic curves, E1L, for the triton lab energy as a function of the proton lab energy. The results in Fig. 5 are consistent with those in Fig. 3.

In Figs. 6 through 9 are the data for the reaction $^{3}He(d,tp)^{1}H$ with 20-MeV incident deuterons. For these and subsequent figures, the projected phase space is plotted explicitly in the dashed curves with an arbitrary scale factor. Note that the data at the top of Fig. 6 deviate distinctly from the shape of the phase space. The additional width and the shift to higher energy of the maximum in the cross section of this resonance, as compared with the lower energy data, may be due to the presence of a third level in ^{4}He at 22.2 MeV as predicted from the phase-shift analysis of scattering data.[14]

In Fig. 7, the same data which were projected along the triton axis in Fig. 6 are projected along the proton axis.

Figure 8 shows additional data for 20-MeV incident deuteron energy. Special attention is directed to arrow R in the middle data plot. This position on the triton axis is significant in that the center-of-mass interaction energies for all three pairs of final-state interactions are approximately the same. This anomaly is also noticeable in the data when they are projected along the proton axis in Fig. 9. Occasionally, small peaks were also noted when only two interaction energies had the same value. In general, however, these effects were not consistent enough to permit verification as real phenomena.

The Reaction $^{2}H(t,tp)n$

The data in Figs. 10 through 13, 15, and 16 are from the reaction $^{2}H(t,tp)n$ with 21-MeV incident tritons. These data are dominated by huge peaks due to the spectator pole-type breakup of the deuteron. Similar direct-reaction type breakup[24] has been observed in the reaction $^{16}O(\alpha,2\alpha)^{12}C$. These peaks were found to occur whenever the laboratory energy of the unobserved third particle (i.e., E3L) goes through a minimum. The detailed kinematics associated with this phenomena are presented in Fig. 14 for the data in Figs. 12 and 13. There are also several peaks due to the asymptotic increase of the projected phase space. In Fig. 15, numbers without parenthesis are representative t + p center-of-mass excitation energies above the ^{4}He ground state. Numbers in parenthesis are representative t + n center-of-mass excitation energies. Figure 16 shows a check made on the consistency of the absolute cross-section determination. The triangles indicate data from a narrow slit system with $\Omega_t = 6.05 \times 10^{-4}$ sr and $\Omega_p = 8.56 \times 10^{-4}$ sr. The dots indicate data taken with a wider slit system with $\Omega_t = 1.26 \times 10^{-3}$ and $\Omega_p = 1.67 \times 10^{-3}$ sr. The difference between the two sets of data is well within the estimated accuracy for the cross-section determination.

The Reaction $^{3}H(d,tp)n$

The data for this reaction are shown in Figs. 17 and 18. The incident deuteron energy, after correction for energy loss in the entrance foil of the gas target, was 20 MeV. The data at the top of Fig. 17 are very similar in overall yield and spectral shape to the $^{3}He(d,tp)^{1}H$ data at the top of Fig. 8. The dashed curve represents the projected phase space plotted on an arbitrary vertical scale. The data at the tops of Figs. 17 and 18 are clearly in disagreement with the shape of the projected phase space. The more or less nondescript data in the two lower sections of Figs. 17 and 18 indicate that the resonant yields at this energy are much more clearly observed at small angles with respect to the incident beam.

SUMMARY

The location and approximate full width at half-maximum as a function of the three possible pairs of final-state center-of-mass excitation energies for all observed peaks are summarized in Figs. 19 and 20. The long lines in these figures denote the center-of-mass excitation energy ranges for the three pairs of particles in the final state. Open boxes denote the approximate full width at half-maximum of the resolvable peaks. Solid boxes represent a double-valued region for the center-of-mass excitation energy. Arrows show the positions of peaks in the cross section, and

dashed arrows indicate the positions of questionable peaks. Each set of angles has a pair of these lines and boxes, with those at the top representing the triton projections and those at the bottom, the proton projections. The energy-level diagrams at the bottoms of the figures are based primarily on phase-shift analysis of scattering data.[14] In Fig. 20, the solid dots at the bases of some of the arrows denote minima in the energy of the unobserved third particle which are associated with direct-reaction spectator poles.

From the combination of the 15- and 20-MeV data for the reaction $^{3}He(d,tp)^{1}H$ in Fig. 19, it is apparent that the observed resonance is in the vicinity of 22 MeV, not at 26 MeV. It is probably coincidental that the positions of the partially resolved structure in some of these resonant peaks match the predictions for the location of the second and third levels[14] in ^{4}He to better than the half-width of these levels. It must be remambered that the position at which the resonant phase shift goes through 90° does not necessarily coincide with the maximum in the resonance cross sections.

The data with 15-MeV incident deuterons have a maximum at 21.5 ± 0.1 MeV, and the corresponding 20-MeV data have a maximum at 22 ± 0.2 MeV above the ^{4}He ground state. The center-of-mass widths of these levels are approximately 1 and 2 MeV, respectively. It is interesting to note that a two-parameter experiment with the reaction $^{2}H(^{3}He,tp)^{1}H$ by Parker et al.[1] yielded a resonance at 21.24 ± 0.2 MeV with a width of 1.1 ± 0.2 MeV. This is to be compared with the results of a one-parameter experiment by Williams[2] in which the reaction $^{4}He(p,p')^{4}He^{*}$ yielded a resonance at 22.00 ± 0.14 MeV with a width of 2.4 ± 0.5 MeV. The data presented in this paper indicate that these differences are due to poorer resolution of the one-parameter experiment.

The data from the reaction $^{2}H(t,tp)n$ is so dominated by the spectator-pole breakup of the deuteron that no reliable interpretation of final-state interactions can be extracted without a detailed theory for the characteristics of this breakup.

The data from the reaction $^{3}H(d,tp)n$ are meager, but there is good evidence at one set of angles for a final-state t + p resonance at about 22 MeV above the ground state of ^{4}He.

Evidence for the existence or nonexistence of resonances at higher energies[11,12,25] was inconclusive. No evidence for rescattering phenomena was observed.[26-28]

ACKNOWLEDGMENTS

The author owes special thanks to G. G. Ohlsen and N. Jarmie for their interest and discussions concerning this work. Special thanks are also due J. S. Levin and M. P. Kellogg for their help with the computer and computer programs. The author also thanks R.L. Henkel, R. Woods, and the rest of the staff of the Los Alamos three-stage Van de Graaff facility for their full cooperation and assistance.

REFERENCES

1. P. D. Parker, P. F. Donovan, J. V. Kane, and J. F. Mollenaur, Phys. Rev. Letters 14, 15 (1965).
2. L. E. Williams, Phys. Rev. 144, 815 (1966).
3. R. W. Zurmühle, Nucl. Phys. 72, 225 (1965).
4. J. Cerny, C. Détraz, and R. H. Pehl, Phys. Rev. Letters 15, 300 (1965).
5. N. Jarmie, R. H. Stokes, G. G. Ohlsen and R. W. Newsome, Jr., Phys. Rev. 161, 1050 (1967).
6. P. G. Young and G. G. Ohlsen, Phys. Letters 8, 124 (1964); 11, 192(E) (1964).
7. B. R. Barrett, Phys. Rev. 154, 955 (1967).
8. A. De-Shalit and J. D. Walecka, Phys. Rev. 147, 763 (1966).
9. Y. C. Tang, Phys. Letters 20, 299 (1966).
10. W. E. Meyerhof, Phys. Rev. Letters 16, 1114 (1966).
11. P. E. Argan, G. C. Mantovani, P. Marazzini, A. Piazzoli, and D. Scannicchio, Nuovo Cimento Suppl. Vol. III, No. 2, 245 (1965).
12. W. E. Meyerhof and T. A. Tombrello, Nucl. Phys. A109, 1 (1968).
13. W. E. Meyerhof and J. N. McElearney, Nucl. Phys. 74, 533 (1965).
14. B. R. Barrett, J. D. Walecka, and W. E. Meyerhof, Phys. Letters 22, 450 (1966).
15. A. B. Kerepin in "Studies of Nuclear Reactions," Lebedev Physics Institute Series 33, 1 (1965).
16. N. Jarmie and R. L. Allen, Phys. Rev. 114, 176 (1959).
17. C. Werntz, Phys. Rev. 128, 1336 (1962).

18. T. A. Tombrello, Phys. Rev. 138, 340 (1965).

19. T. A. Tombrello, Phys. Rev. 143, 772 (1966).

20. R. W. Newsome, Jr., Bull. Am. Phys. Soc. 12, 17 (1967).

21. R. H. Stokes, Rev. Sci. Instr. 31, No. 7, 768 (1960).

22. G. G. Ohlsen, Nucl. Instr. Methods 37, No. 2, 240 (1965).

23. E. A. Silverstein, Nucl. Instr. Methods 4, 53 (1959).

24. P. F. Donovan, J. V. Kane, C. Zupancic, C. P. Baker, and J. F. Mollenaur, Phys. Rev. 135, B61 (1964).

25. H. Hänsgen, H. Pose, G. Schirmer, and D. Seeliger, Nucl. Phys. 73, 417 (1965).

26. C. Kacser and I. J. R. Aitchison, Rev. Mod. Phys. 37, No. 3, 350 (1965).

27. I. J. R. Aitchison and C. Kacser, Phys. Rev. 142, No. 4, 1104 (1966).

28. I. J. R. Aitchison, Nuovo Cimento, Vol. LIA No. 2, 272 (1967).

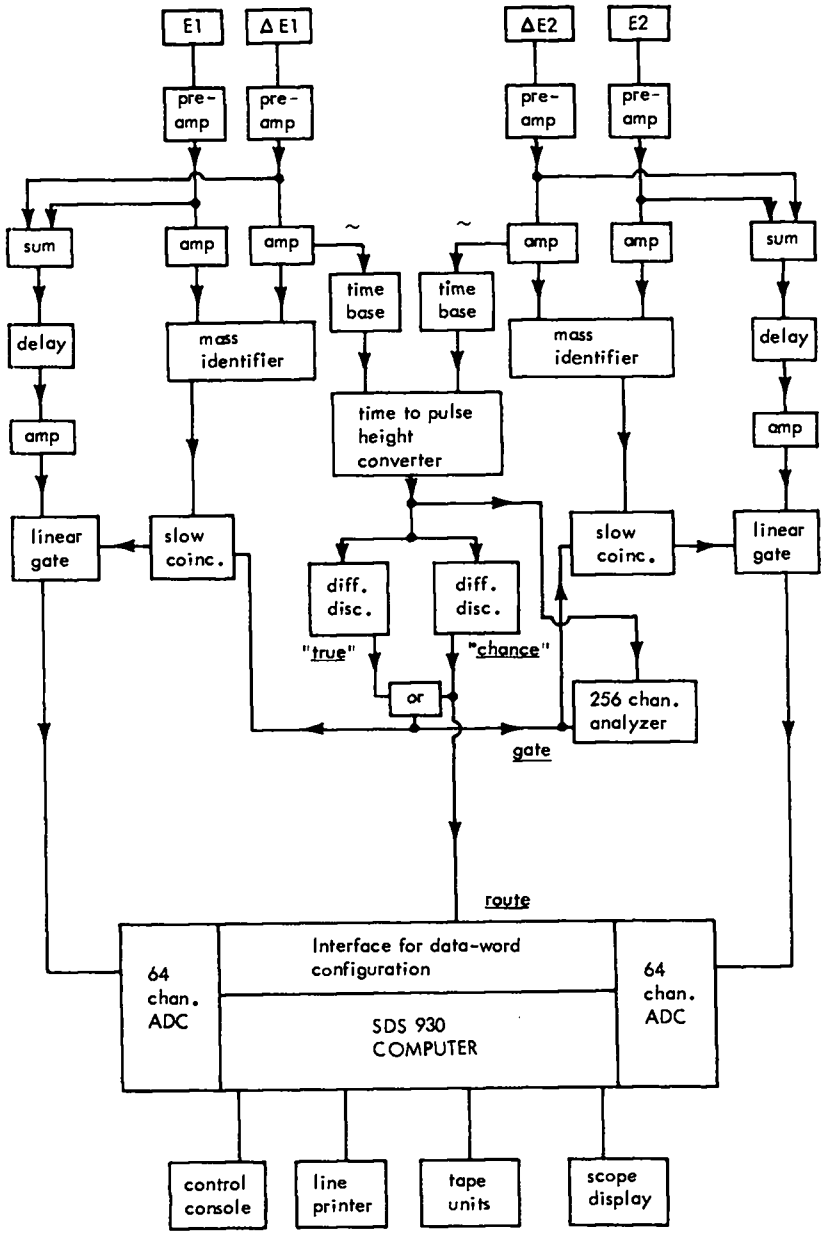

Fig. 1. Schematic of the electronics.

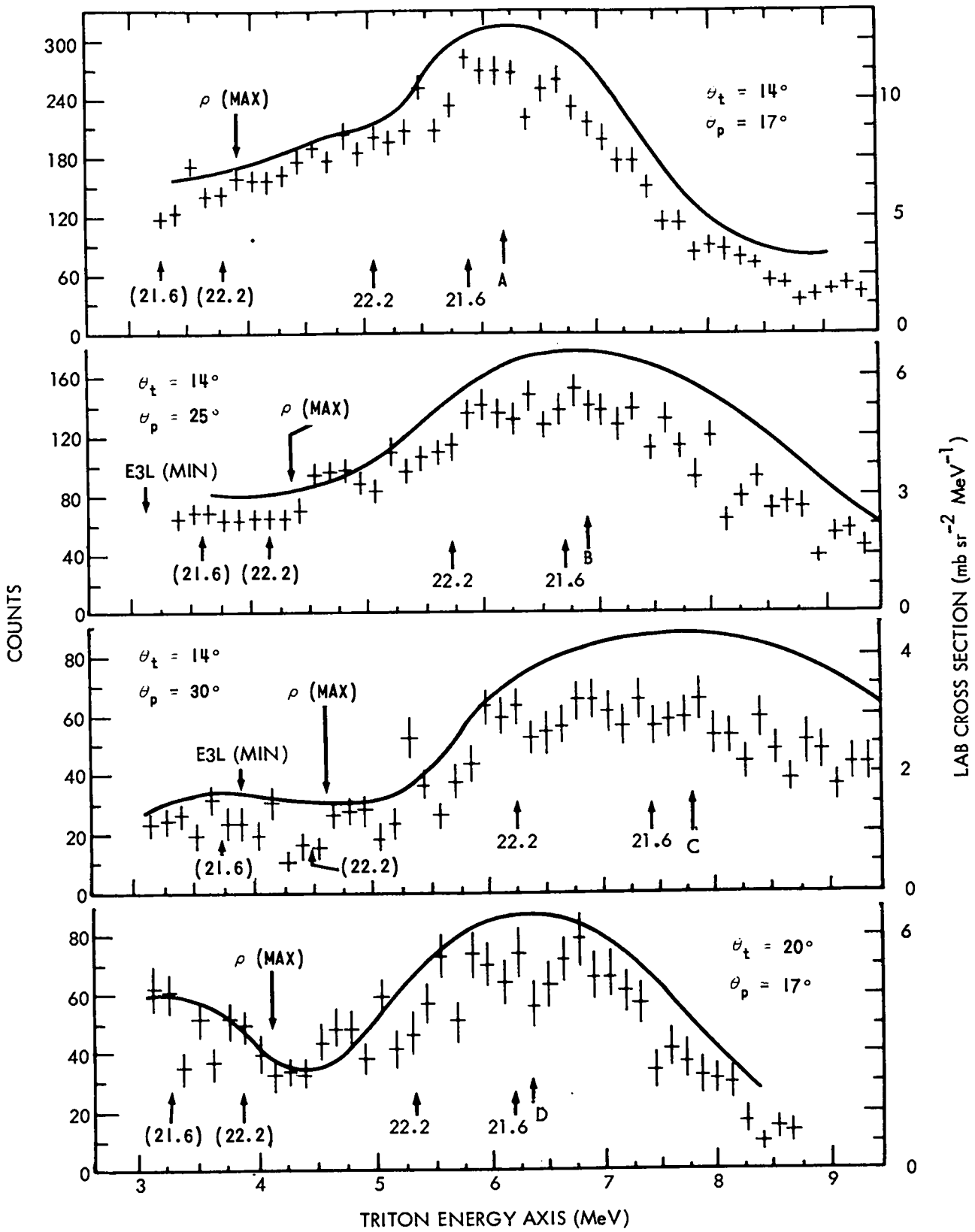

Fig. 2. Projection along the triton lab-energy axis of data from the reaction $^{3}He(d,tp)^{1}H$ with 15-MeV incident deuterons.

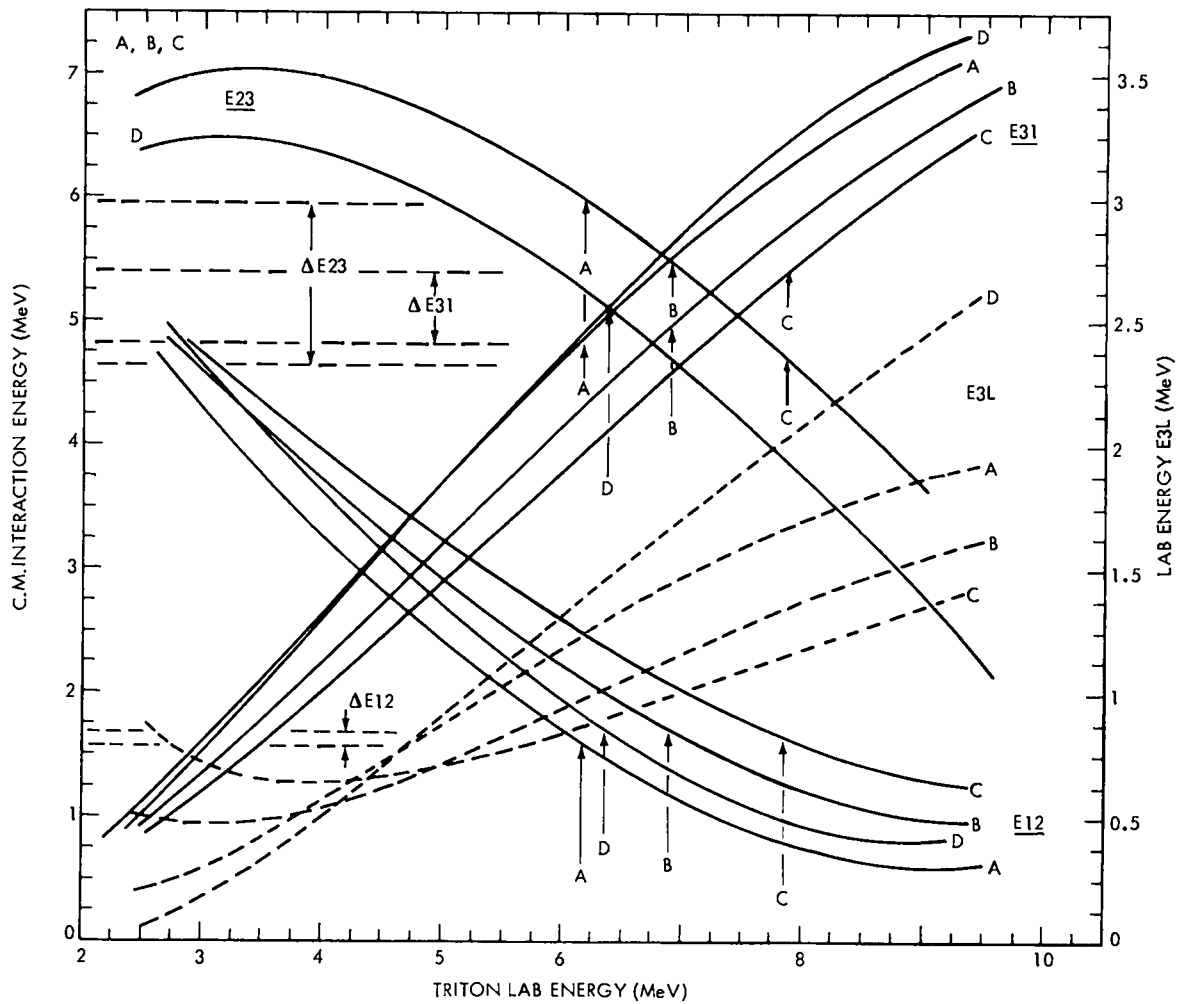

Fig. 3. Kinematics of the data projected along the triton axis in Fig. 2.

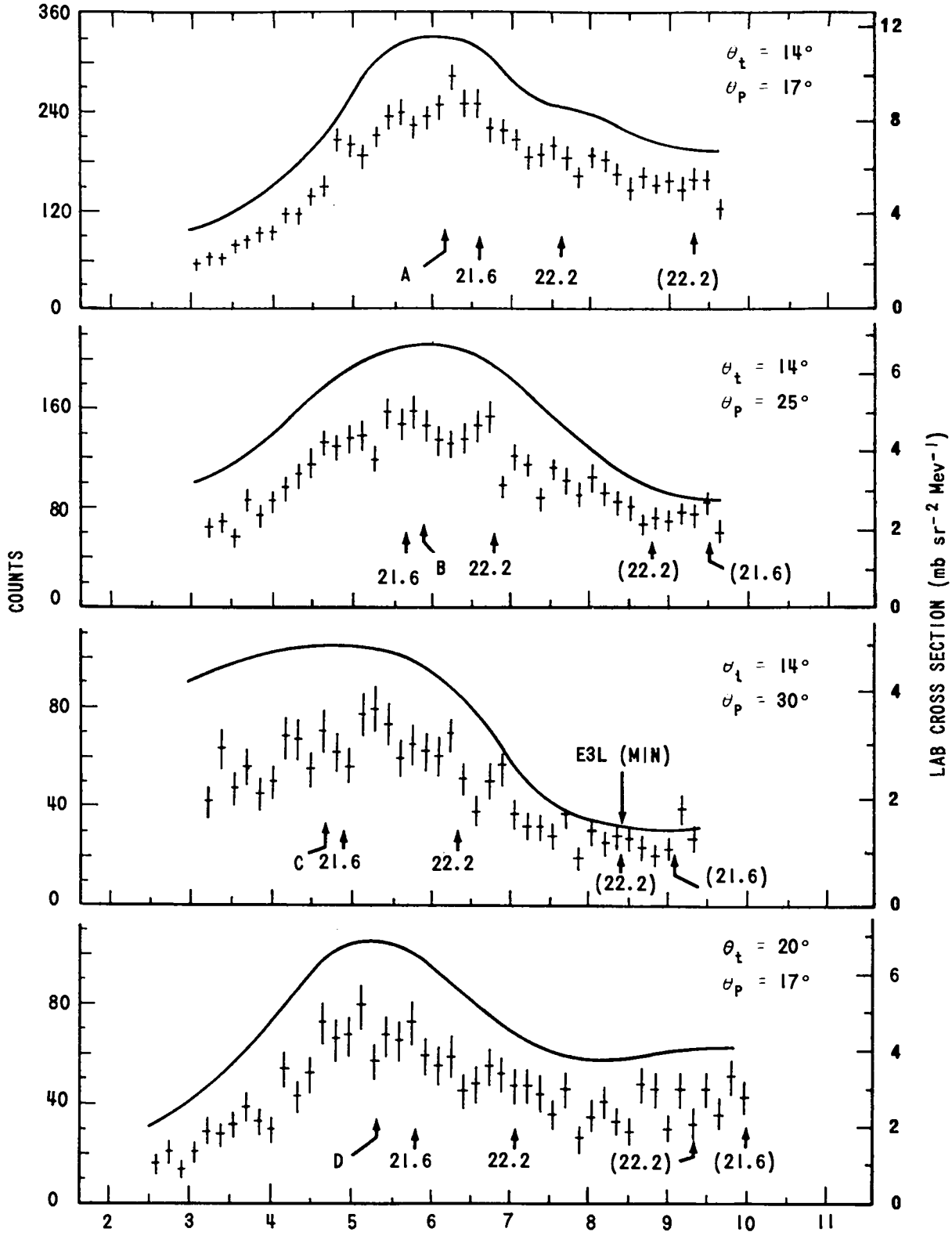

Fig. 4. Projection along the proton lab-energy axis of data from the reaction $^{3}He(d,tp)^{1}H$ with 15-MeV incident deuterons.

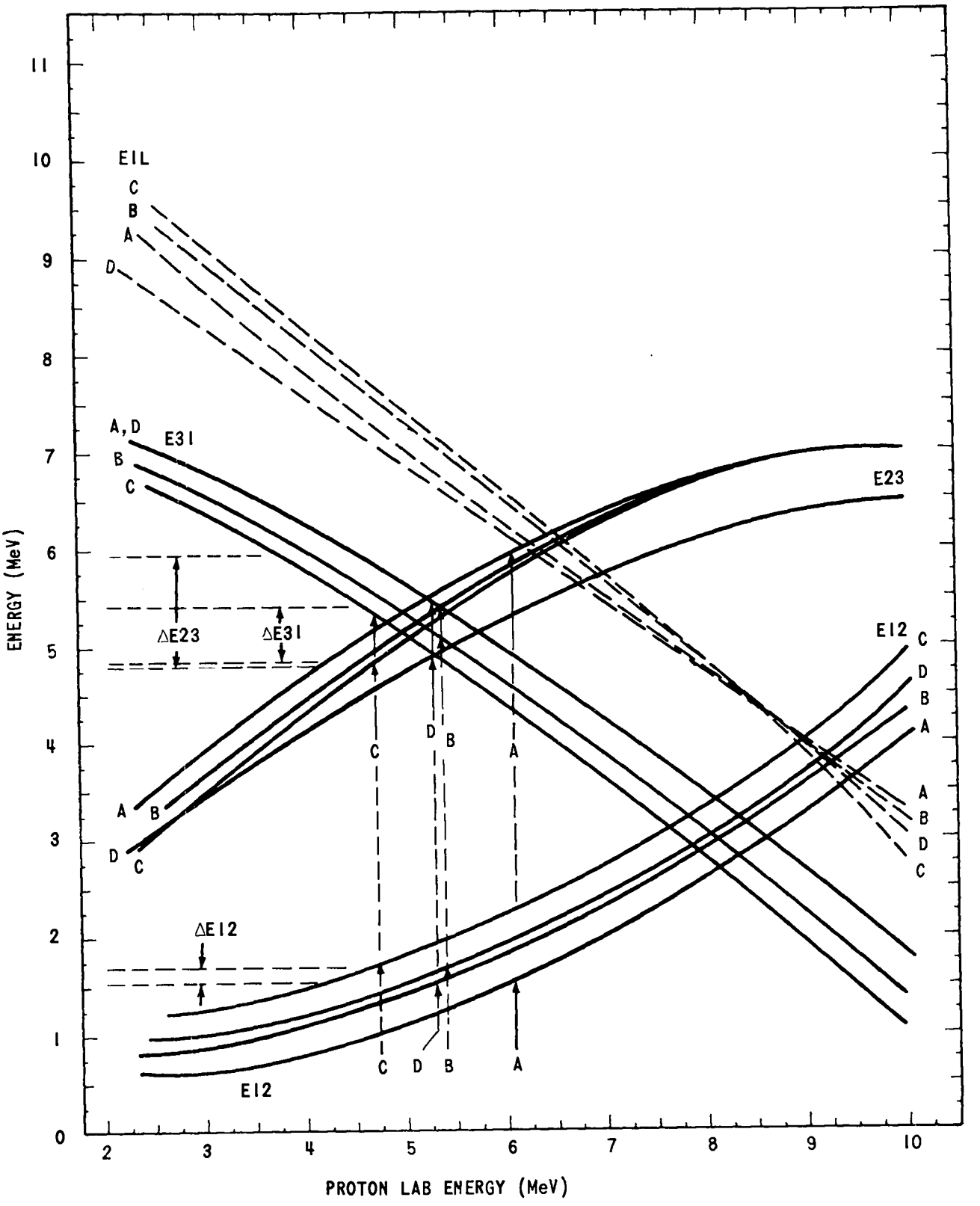

Fig. 5. Kinematics of the data projected along the proton axis in Fig. 4.

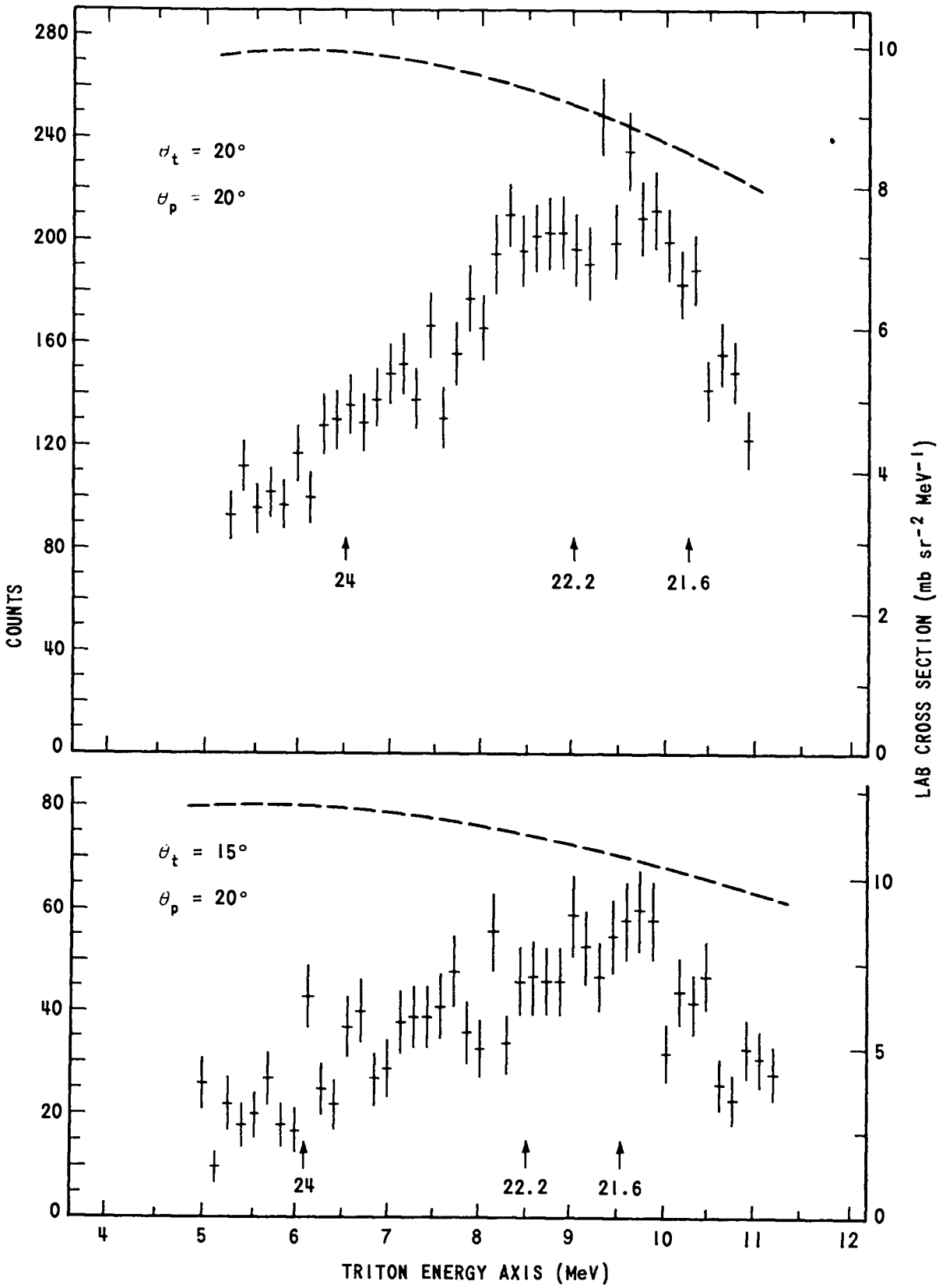

Fig. 6. Projection along the triton lab-energy axis of data from the reaction $^{3}He(d,tp)^{1}H$ with 20-MeV incident deuterons.

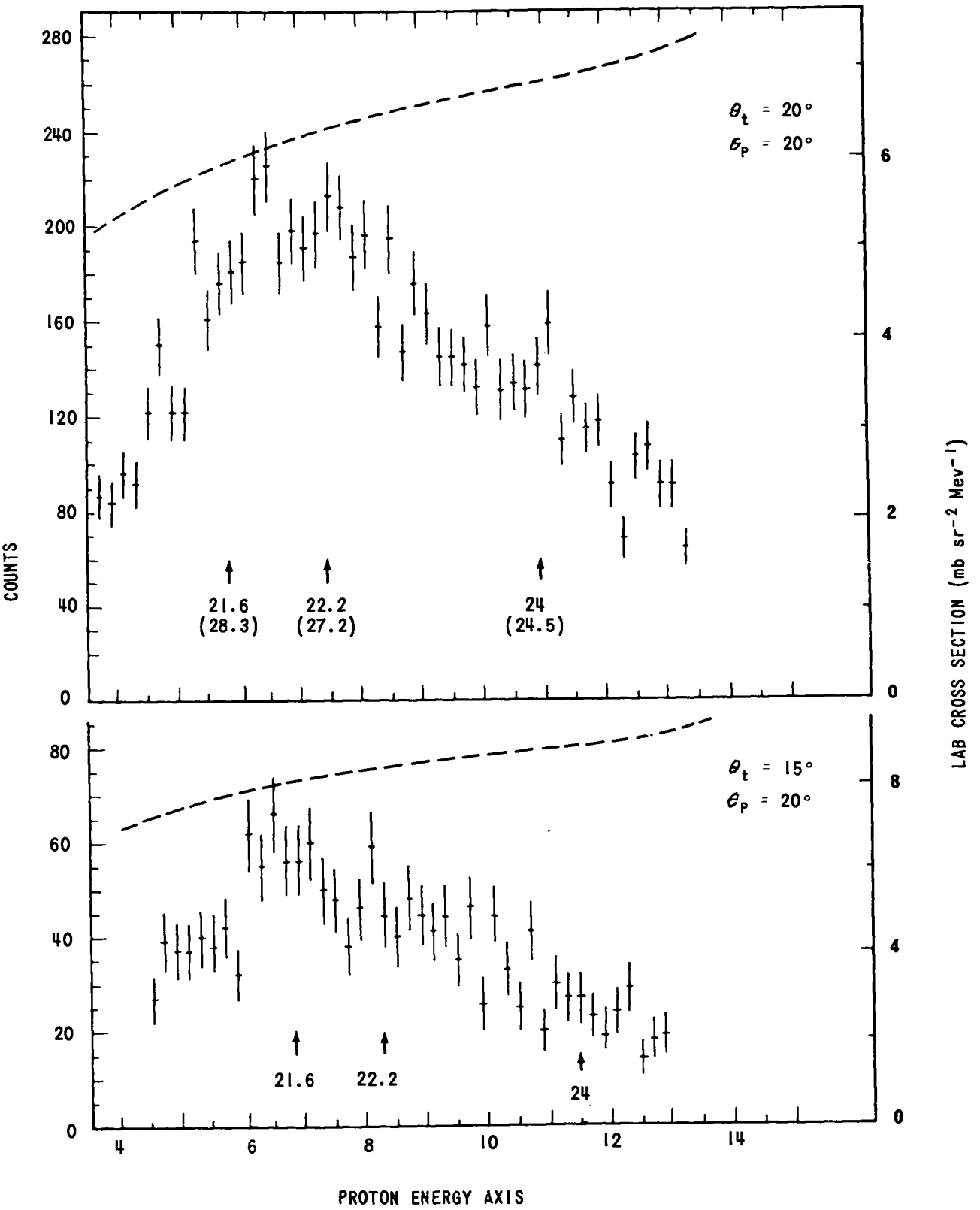

Fig. 7. Projection along the proton lab-energy axis of data from the reaction $^{3}He(d,tp)^{1}H$ with 20-MeV incident deuterons.

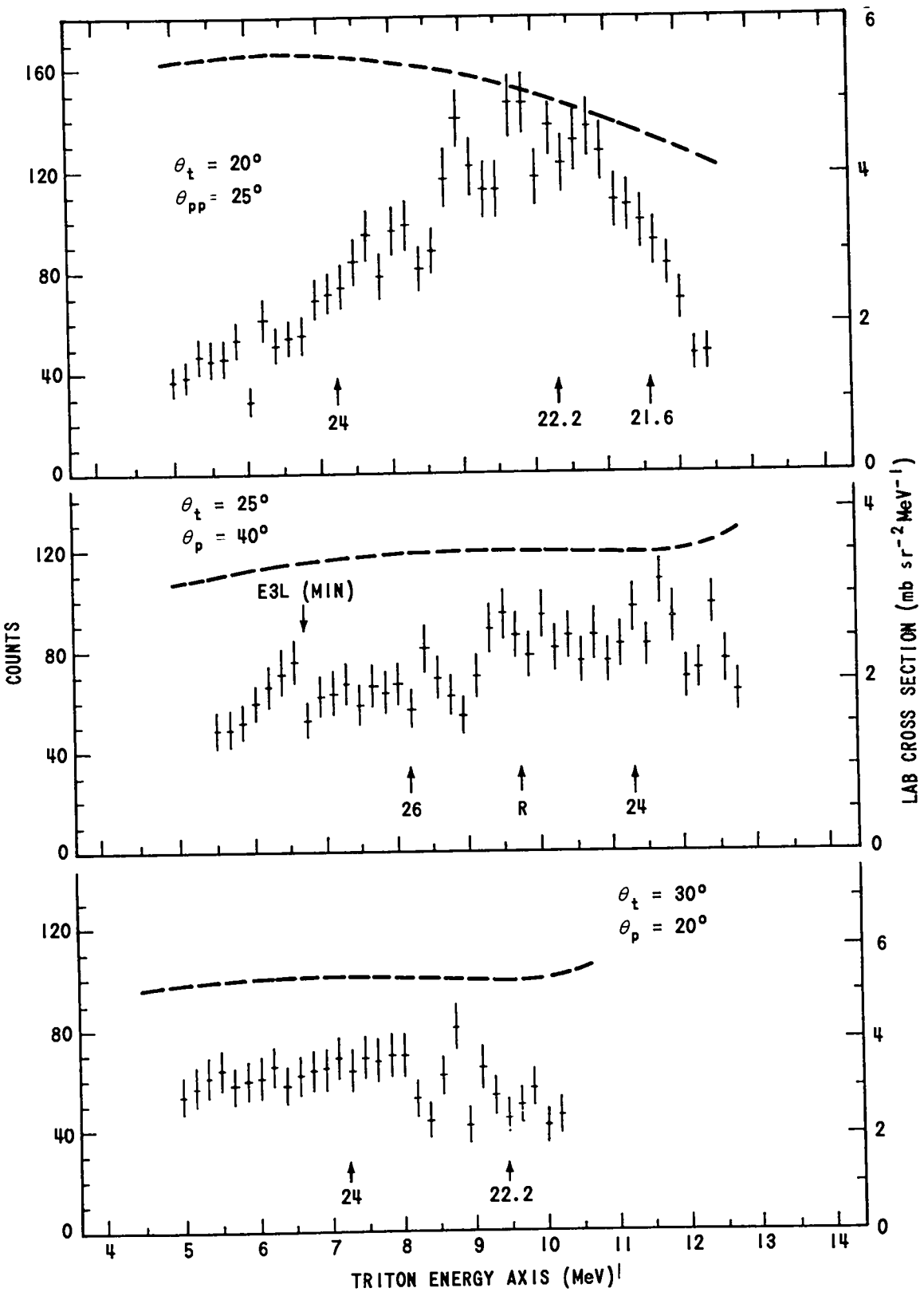

Fig. 8. Projection along the triton axis of additional data from the reaction $^3He(d,tp)^1H$ with 20-MeV incident deuterons.

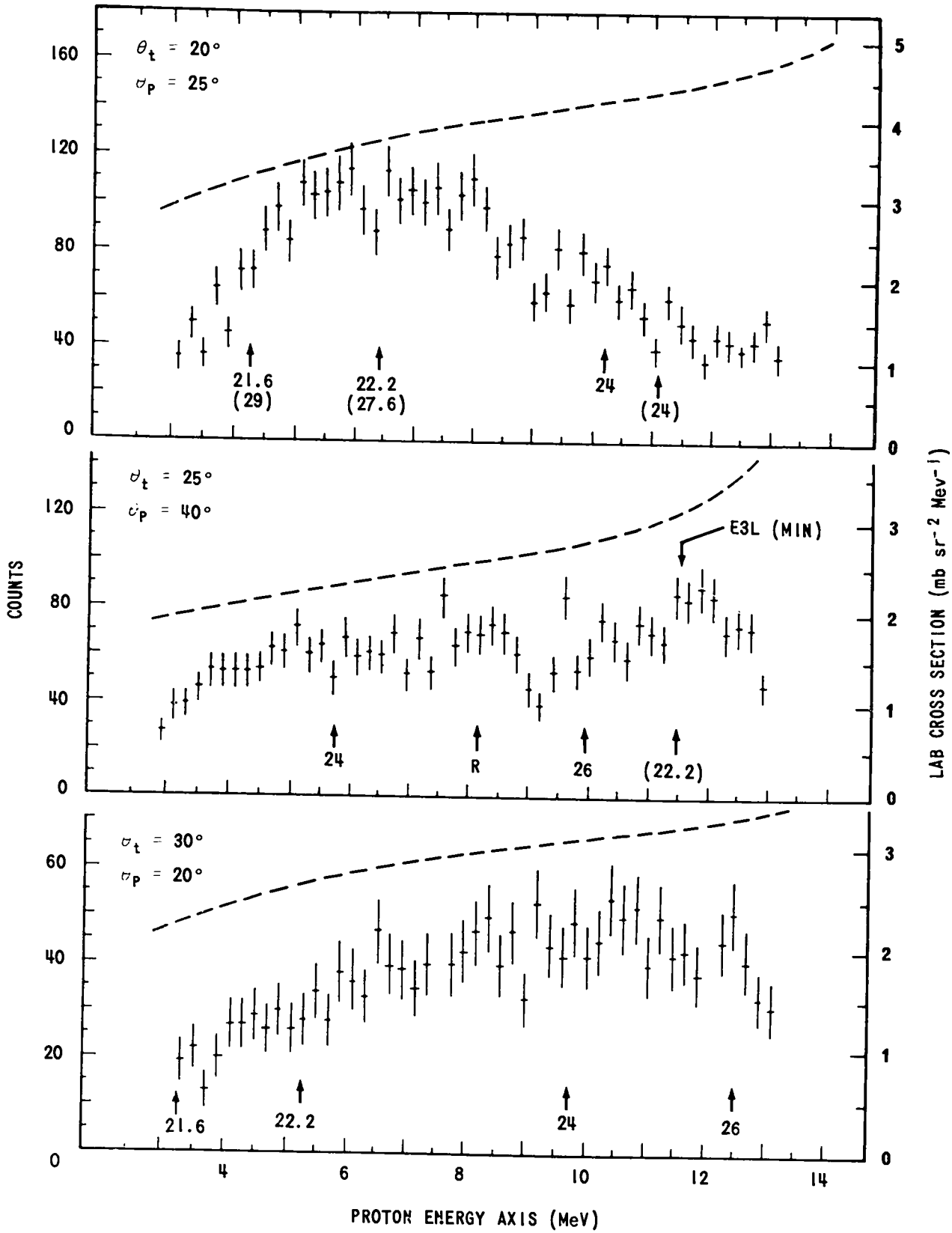

Fig. 9. Projection along the proton axis of additional data from the reaction $^{3}He(d,tp)^{1}H$ with 20-MeV incident deuterons.

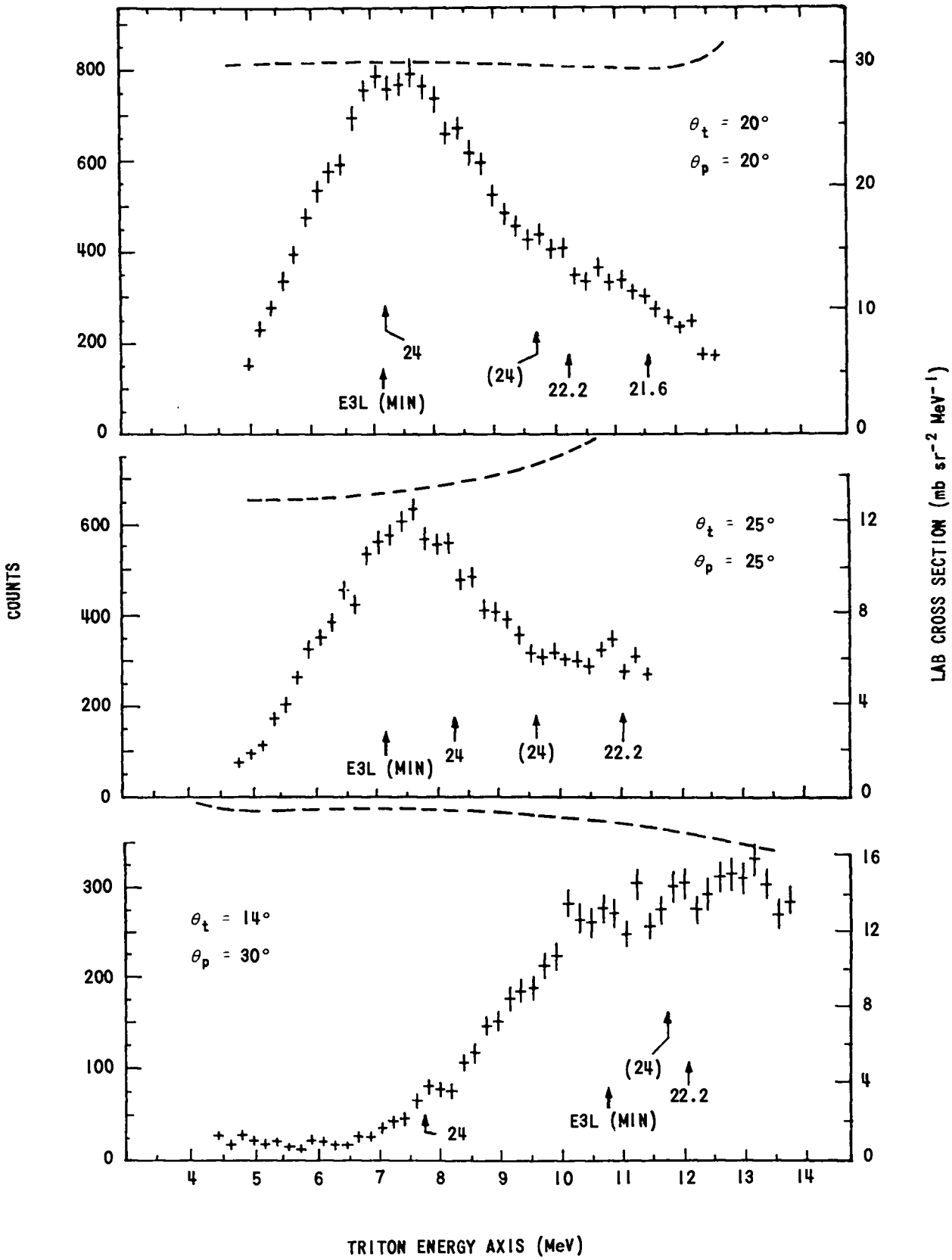

Fig. 10. Projection along the triton lab-energy axis of data from the reaction ^{2}H(t,tp)n with 21-MeV incident tritons.

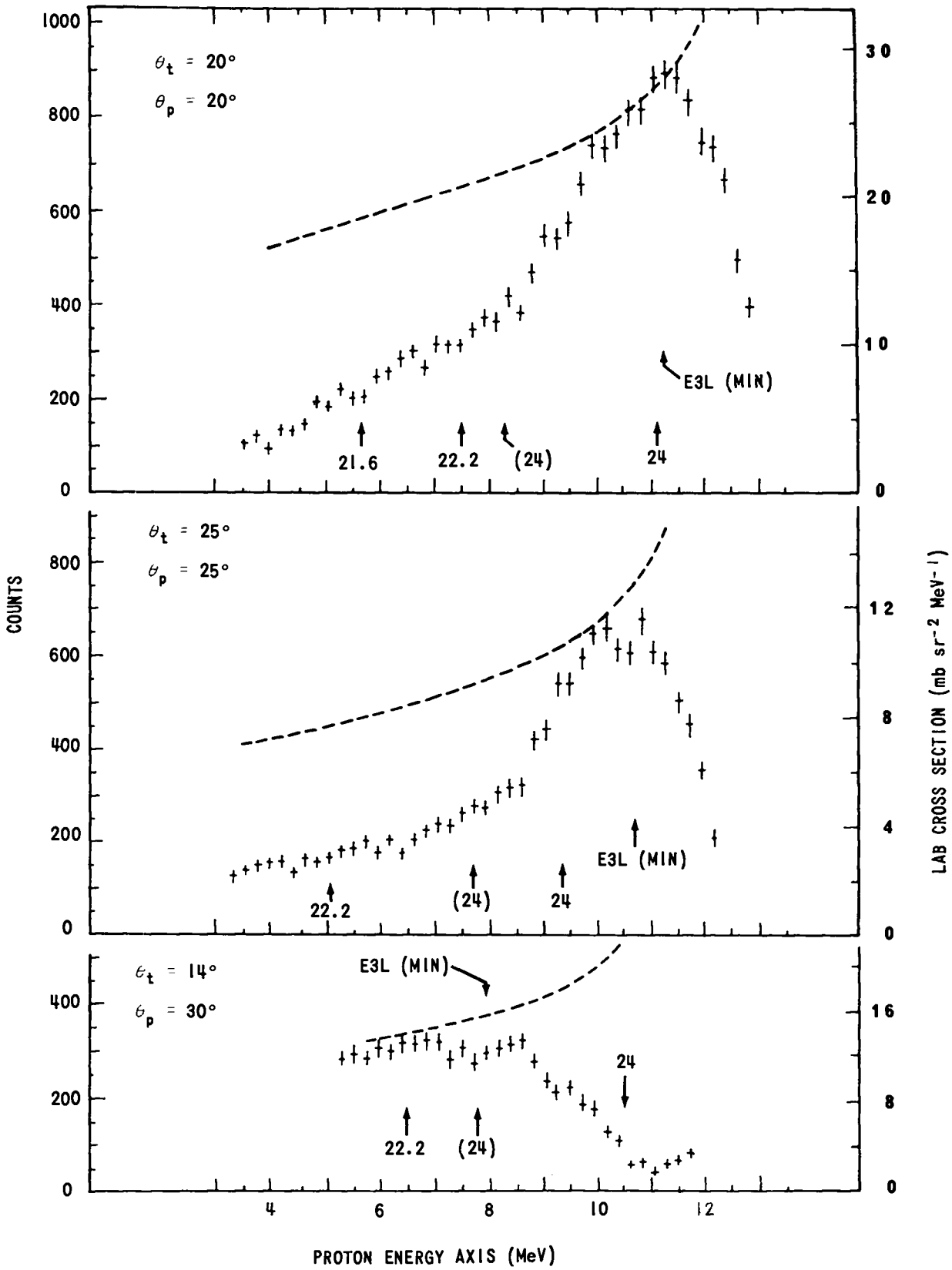

Fig. 11. Projection along the proton lab-energy axis of data from the reaction $^{2}H(t,tp)n$ with 21-MeV incident tritons.

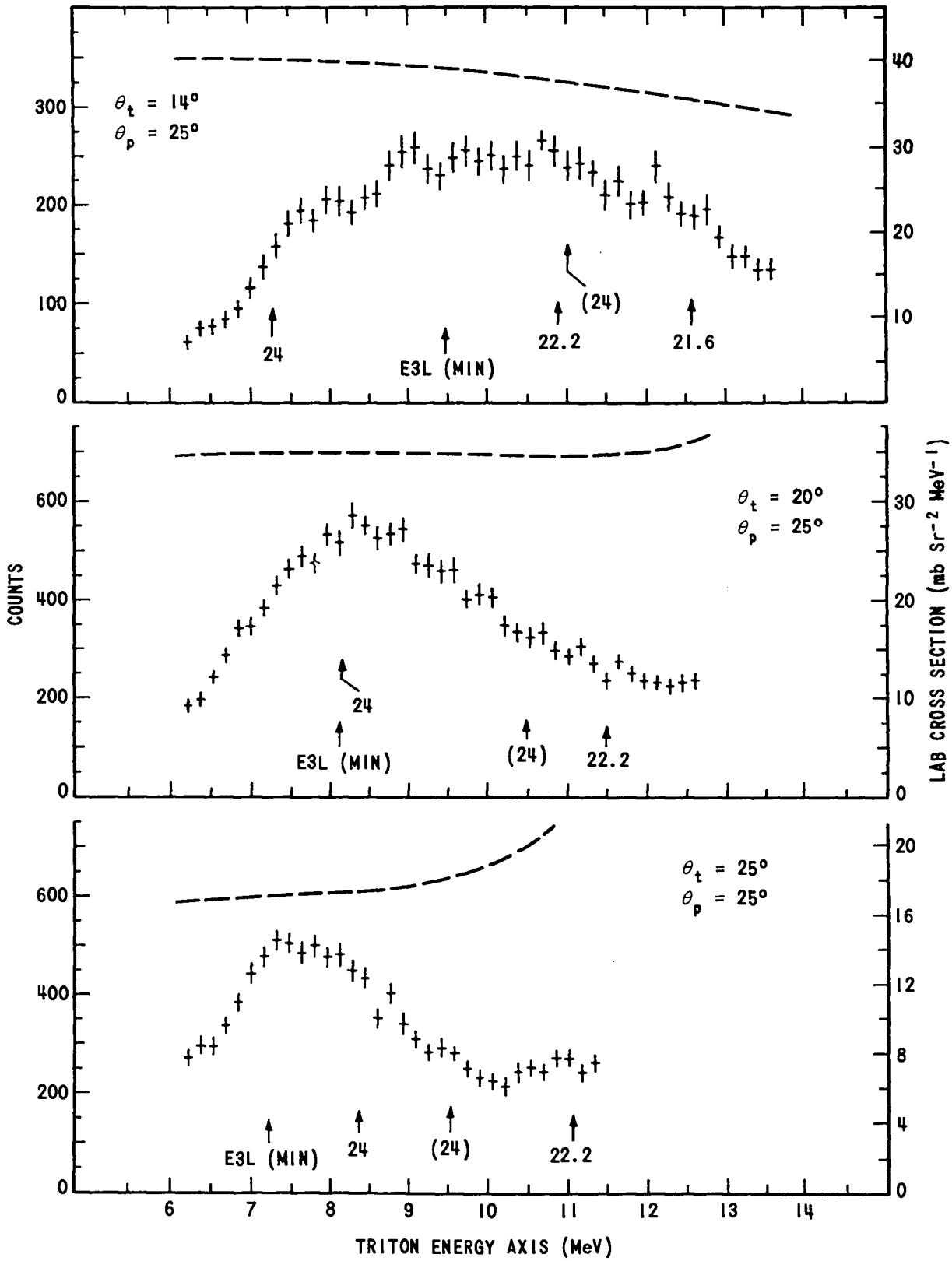

Fig. 12. Projection along the triton axis of additional data from the reaction $^{2}H(t,tp)n$ with 21-MeV incident tritons.

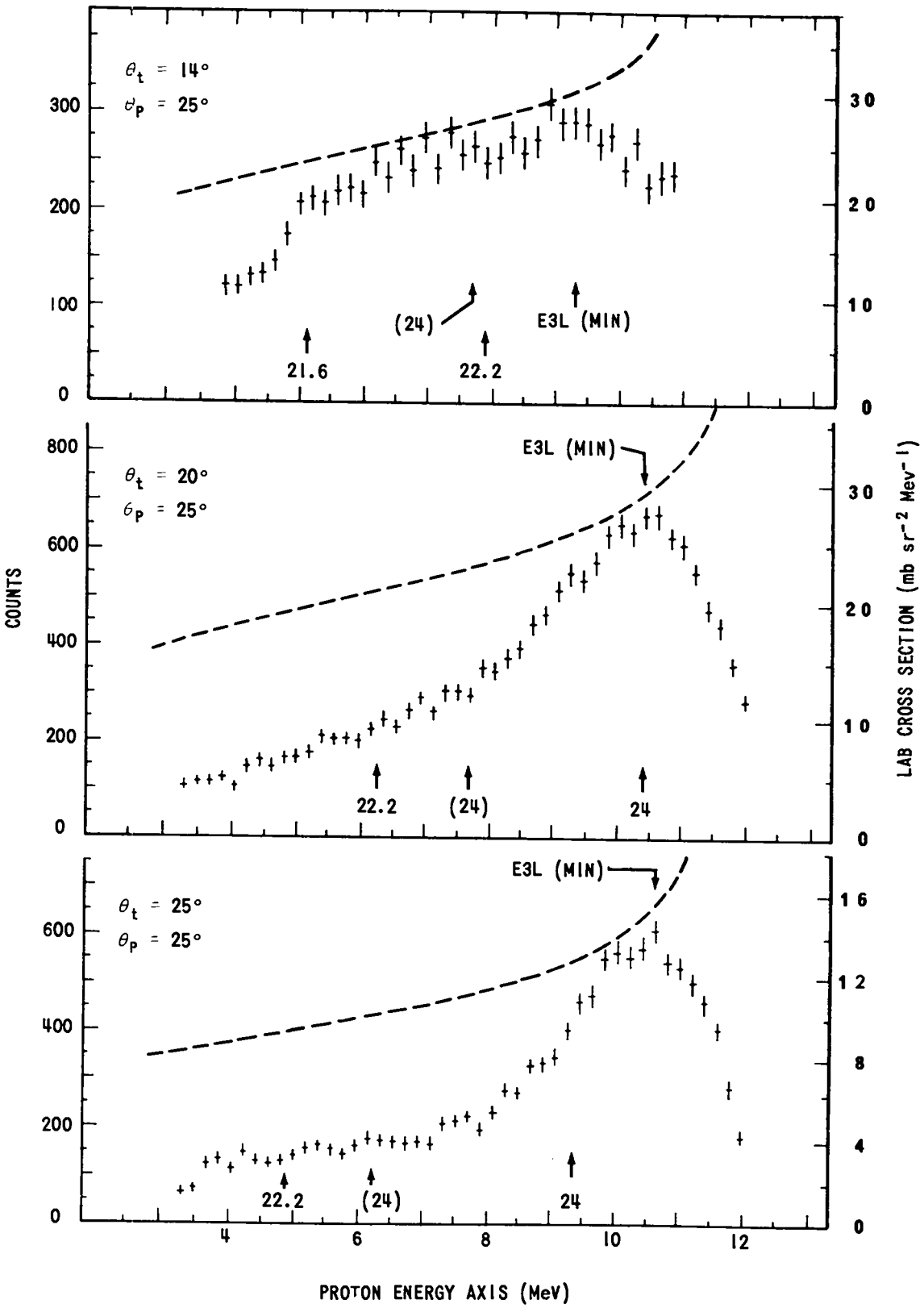

Fig. 13. Projection along the proton axis of additional data from the reaction $^{2}H(t,tp)n$ with 21-MeV incident tritons.

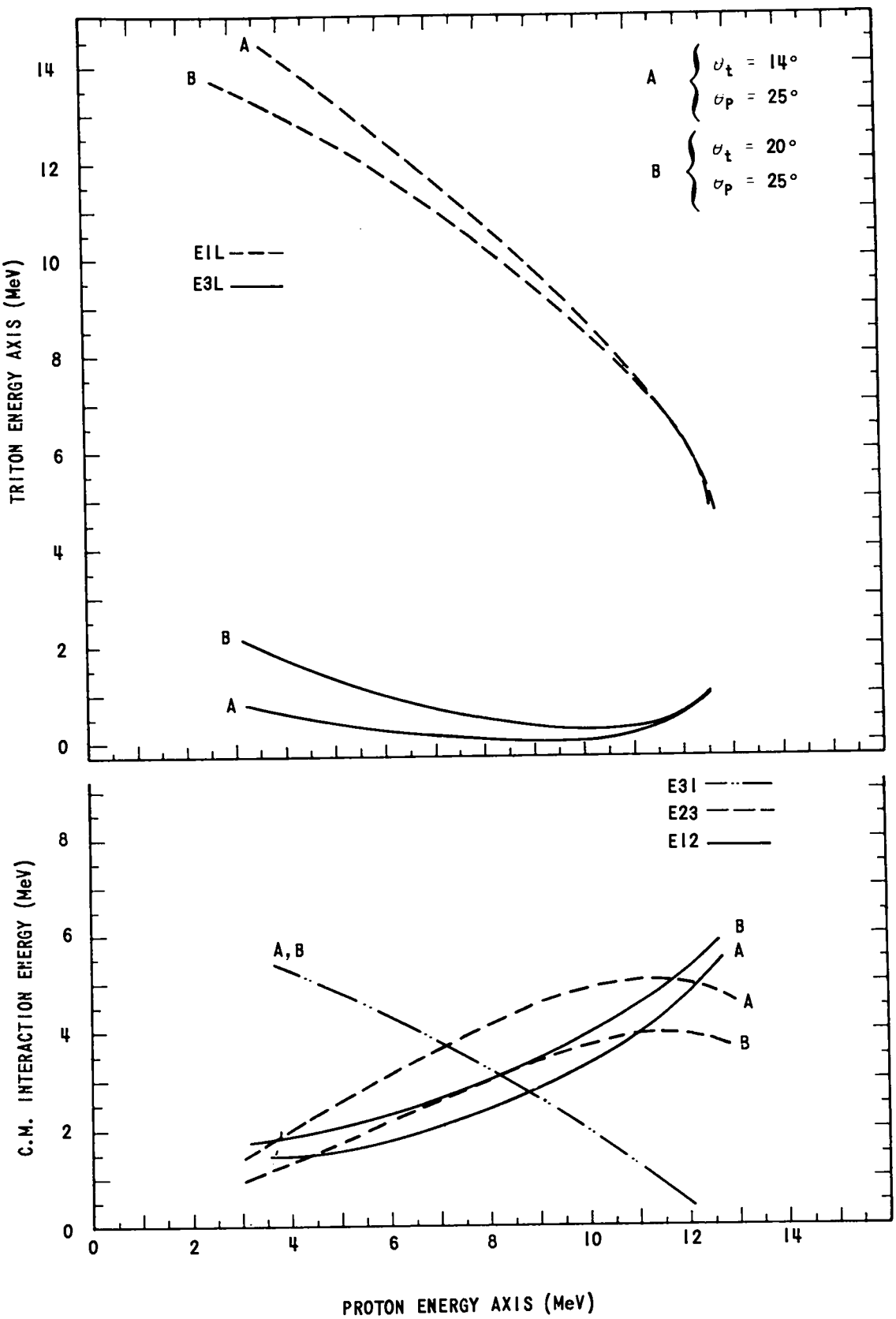

Fig. 14. Kinematics of the first two sets of angles shown in Figs. 12 and 13.

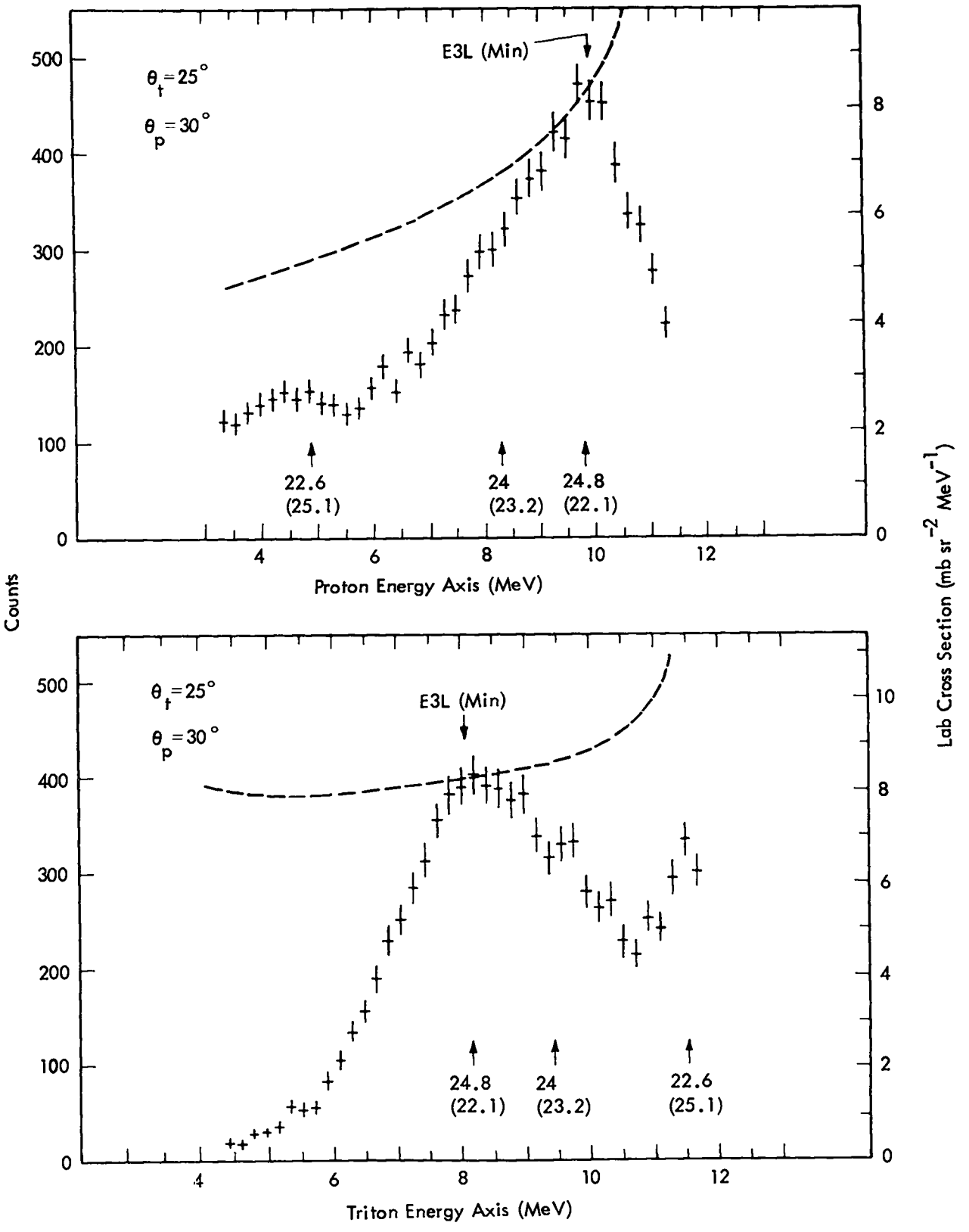

Fig. 15. Projections along the proton and triton lab-energy axes of data from the reaction $^2H(t,tp)n$ with 21-MeV incident tritons.

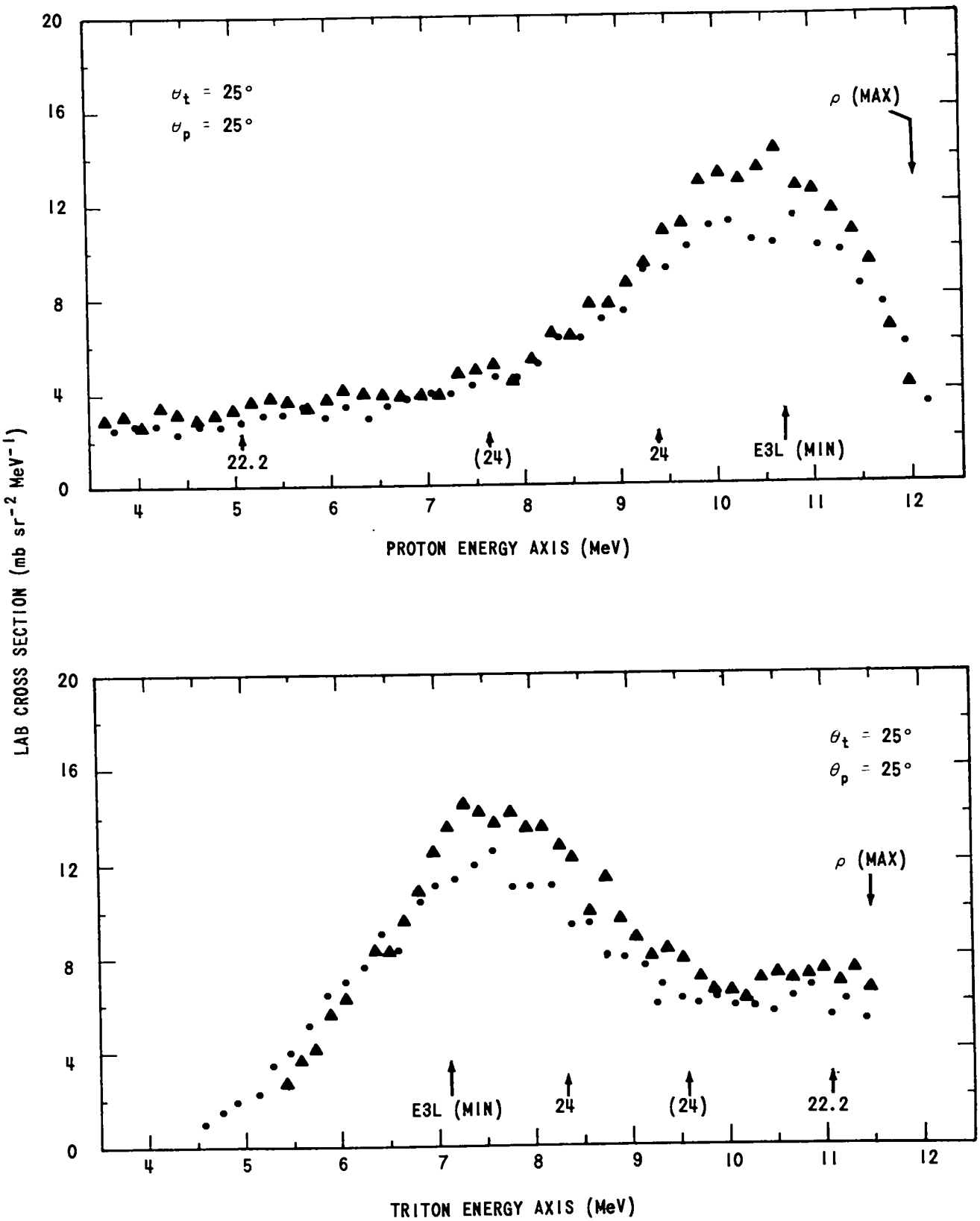

Fig. 16. Projections along the proton and triton axes of data from the reaction ^{2}H(t,tp)n with 21-MeV incident tritons. Same set of angles as in Fig. 15, but significantly different detector solid angles.

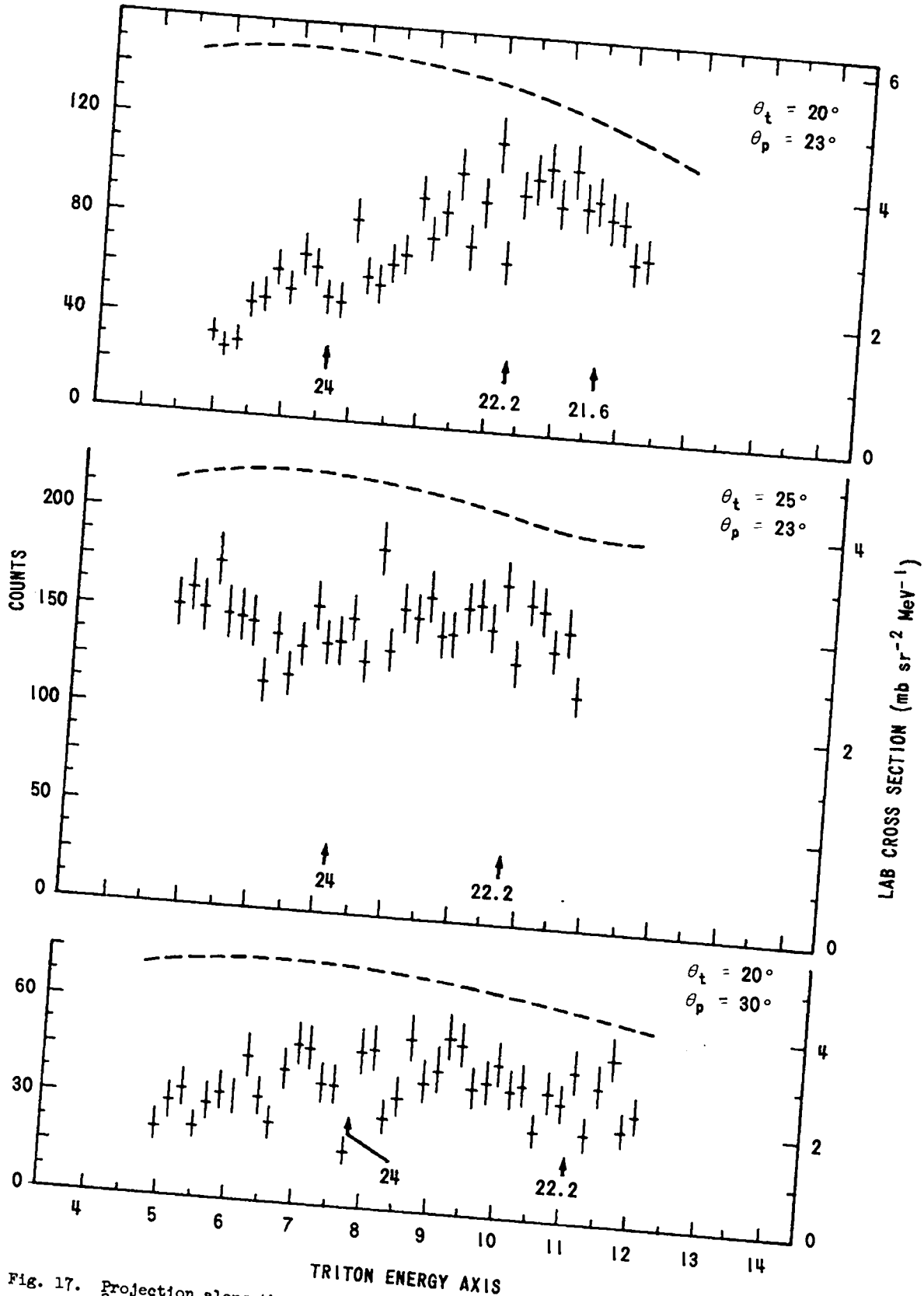

Fig. 17. Projection along the triton lab-energy axis of data from the reaction ^{3}H(d,tp)n with 20-MeV incident deuterons.

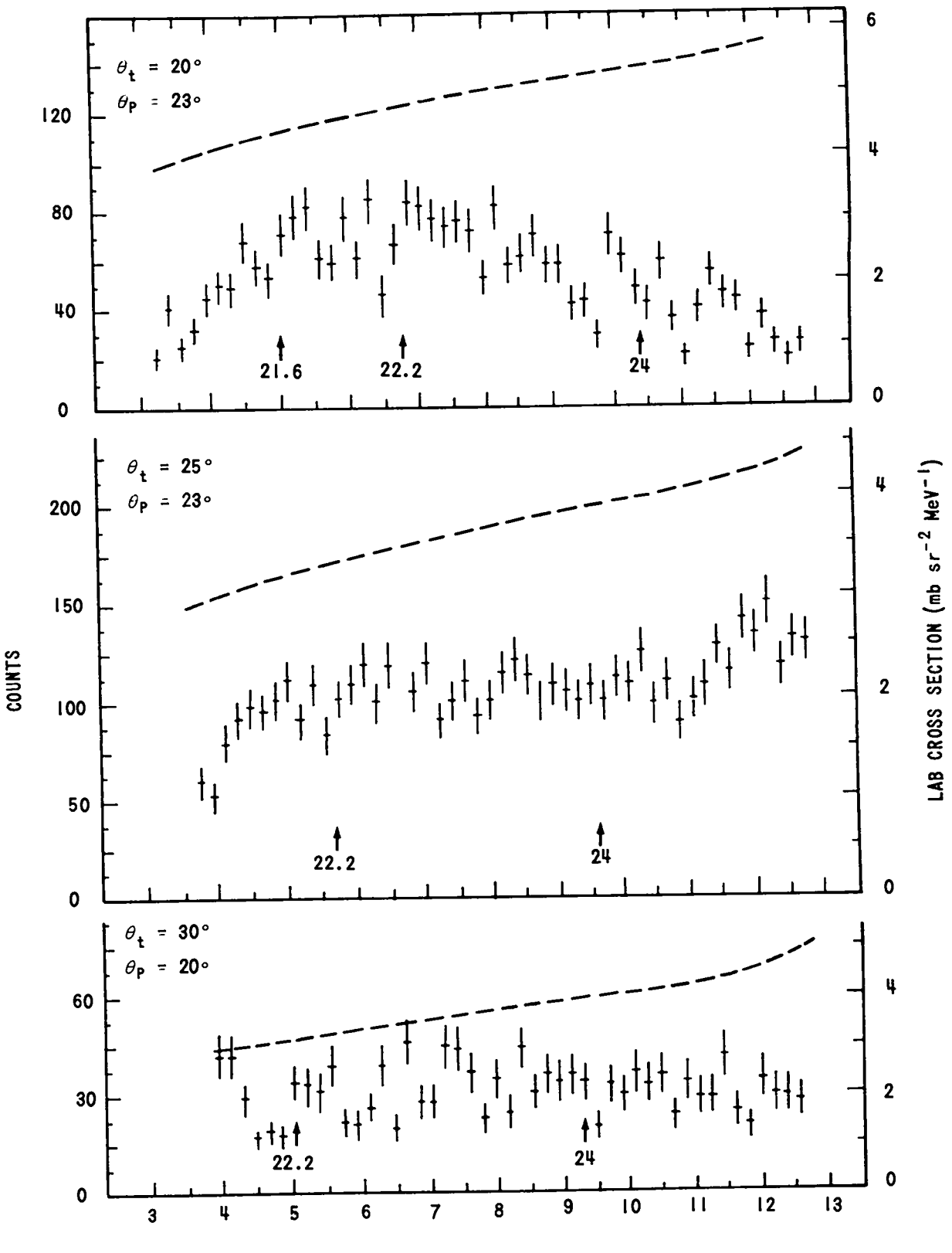

Fig. 18. Projection along the proton lab-energy axis of data from the reaction $^{3}H(d,tp)n$ with 20-MeV incident deuterons.

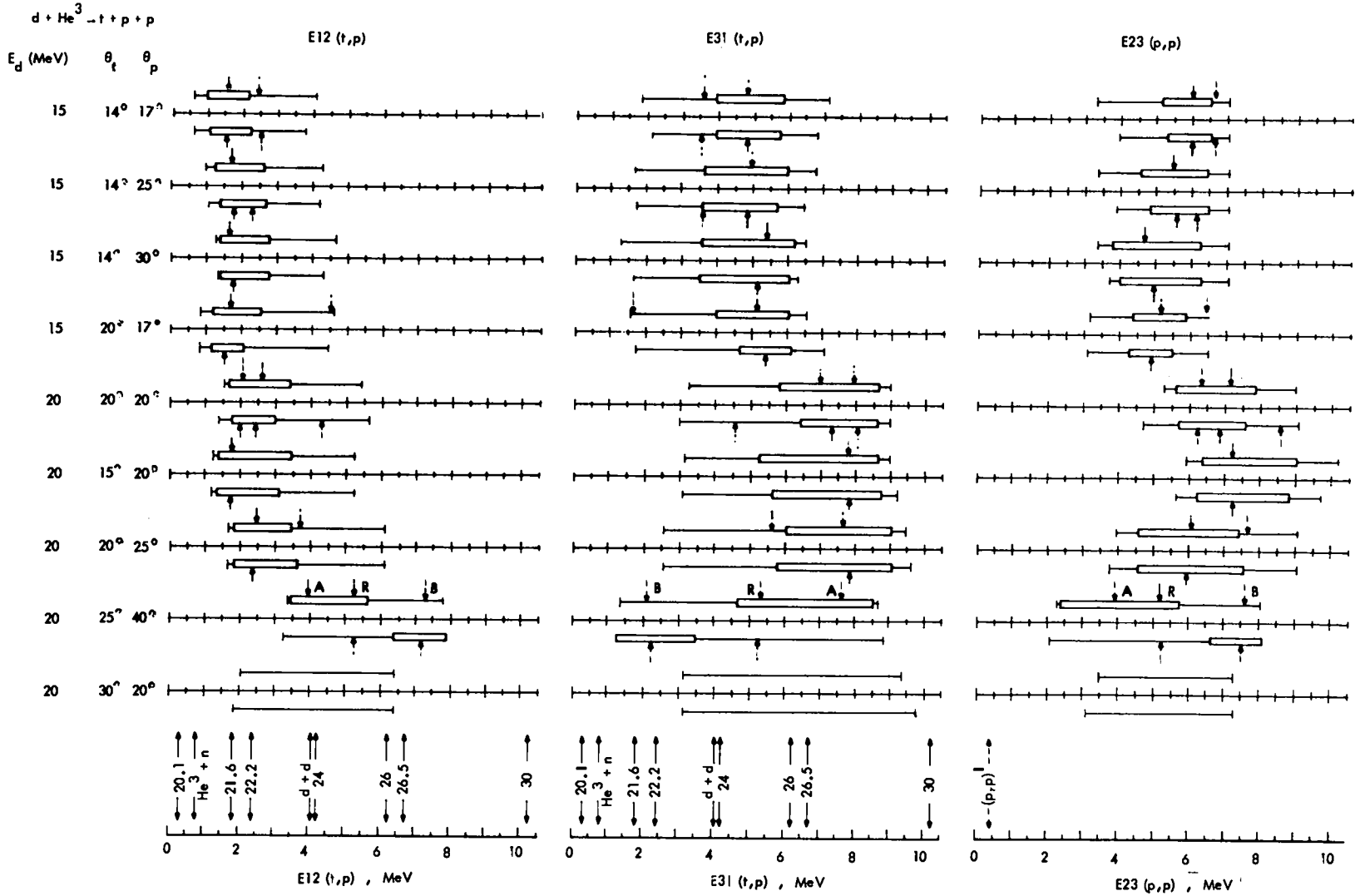

Fig. 19. Graphical summary of the center-of-mass excitation energy information obtained from the $^{3}He(d,tp)^{1}H$ data.

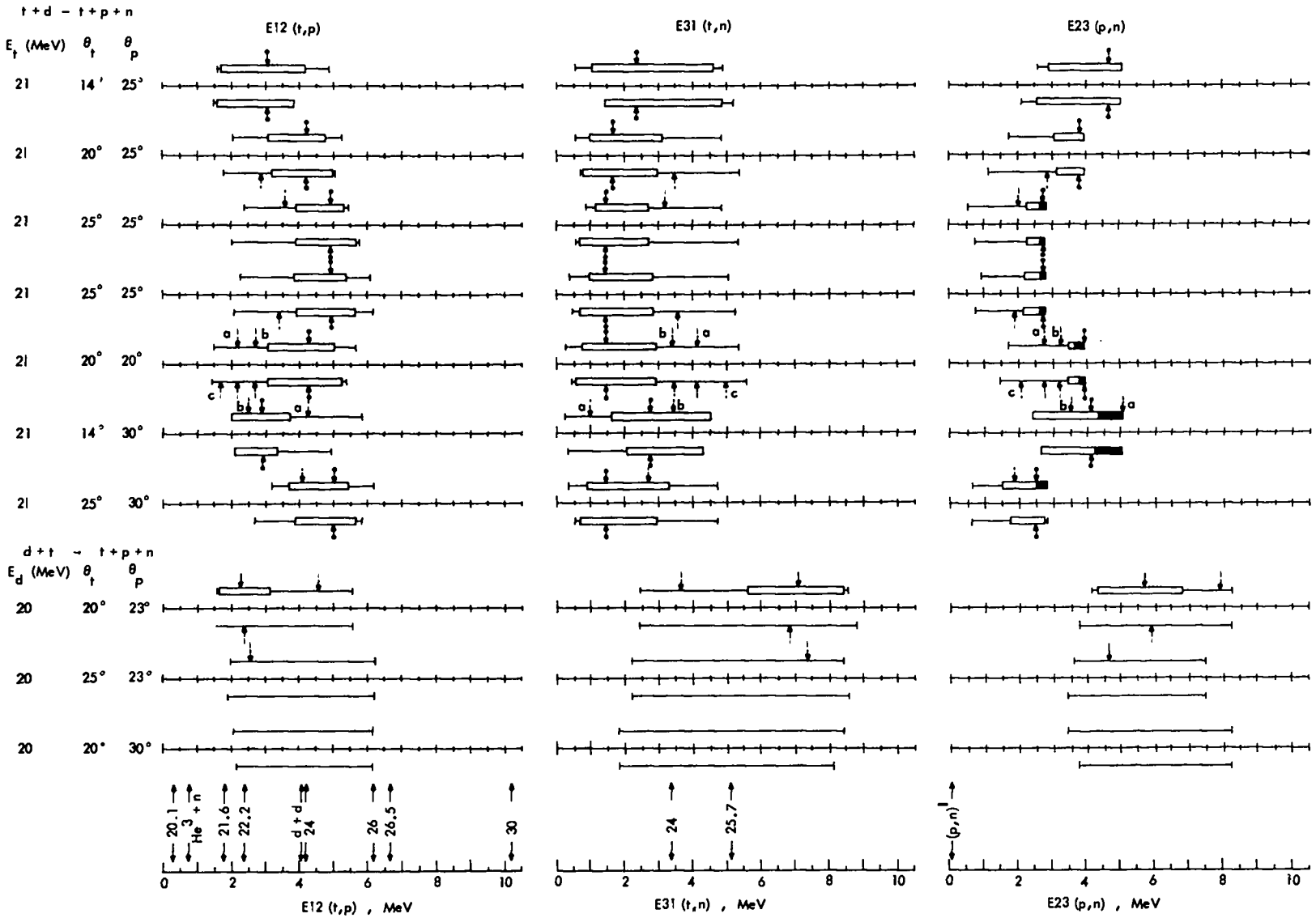

Fig. 20. Graphical summary of the center-of-mass excitation energy information obtained from the $^{2}H(t,tp)n$ and $^{3}H(d,tp)n$ data.